Room temperature processing of TiO_x electron transporting layer for perovskite solar cells

Xiaoyu Deng[1a], George C. Wilkes[2a], Alexander Z. Chen[1], Narasimha S. Prasad[3], Mool C. Gupta [2b], Joshua J. Choi[1b]

1. Department of Chemical Engineering, University of Virginia, Charlottesville, Virginia 22904, USA
2. Department of Electrical and Computer Engineering, University of Virginia, Charlottesville, Virginia 22904, USA
3. NASA Langley Research Center, Hampton, VA 23666

a. These authors contributed equally to this work
b. Correspondence and requests for materials should be addressed to J. J. C and M. C. G. (email: jjc6z@virginia.edu; mgupta@virginia.edu)

Abstract

In order to realize high-throughput roll-to-roll manufacturing of flexible perovskite solar cells, low temperature processing of all device component must be realized. However, the most commonly used electron transporting layer is based on TiO_2 thin films processed at high temperature (>450°C). Here, we demonstrate room temperature solution processing of TiO_x layer that performs as well as the high temperature TiO_2 layer in perovskite solar cells, as evidenced by a champion solar cell efficiency of 16.3%. Using optical spectroscopy, electrical measurements and X-ray diffraction, we show that the room temperature processed TiO_x is amorphous with organic residues and yet their optical and electrical properties are on par with the high temperature TiO_2. Flexible perovskite solar cells, that employ the room temperature TiO_x layer, with power conversion efficiency of 14.3% are demonstrated.

Introduction

Metal halide perovskite (MHP) solar cells have demonstrated the most rapid improvement in power conversion efficiency (PCE) among all photovoltaic technologies to date. With a record PCE of 22.1%,[1] MHP solar cells are now on par with silicon solar cells in terms of efficiency. Moreover, MHP solar cells can be fabricated entirely using low-cost solution processing methods and earth-abundant compositions. Therefore, they can combine high efficiency with low-cost and have a great potential at realizing more economically competitive solar power.

What is particularly exciting about MHPs is that they can be deposited on various substrates, have low processing temperature (< 150 ºC), and enable roll-to-roll manufacturing of low-cost, lightweight and flexible devices.[2] Lead halide based MHPs have been shown to possess a large extinction coefficient greater than 10^4 cm^{-1}, and a long electron-hole diffusion length in the range of hundreds of nm to microns in polycrystalline thin films.[3] This means that only about a 500 nm thick film can harvest most of the sunlight and efficiently transport the photogenerated charges into the external circuit. Such a thin MHP film is highly flexible and corresponds to only 2 g/m^2 of weight which is two orders of magnitude lighter than silicon solar cell. Successful development of MHP solar cells that simultaneously combine high-efficiency, low-cost, lightweight and

flexibility can enable novel portable power generation capabilities in situations where conventional rigid and heavy solar cells are not feasible such as wearable electronics, solar aviation, automobiles, building integrated photovoltaics, etc.

While the quest for achieving high PCE has shown exceptional progress, a majority of the high performance MHP solar cell structures rely on titanium dioxide (TiO_2) electron transporting layer (ETL) processed at high temperatures (>450 °C). The high temperature requirement prohibits the use of flexible plastic substrates such as polyethylene terephthalate (PET) and polyethylene naphthalate (PEN) that cannot withstand temperatures greater than 150 °C. Due to the high performance of metal oxide based ETL for MHP solar cells, it is of great interest to achieve low temperature processing of metal oxide thin films with favorable optical and electrical properties. Indeed, among all flexible MHP solar cell results to date, device architectures that employ metal oxide ETL currently hold the best PCE records of between 15% to 18%[4-6]. Previous efforts to deposit metal oxide ETL on flexible substrates at low temperature have been based on solution processing of nanoparticles,[5,7-13] sputter deposition,[4,14,15] spray coating,[16,17] e-beam evaporation[18], atomic layer deposition,[19,20] and electrodeposition[21,22]. Despite the encouraging device performance, these methods require vacuum processing steps, nanoparticle formulations, etc. that can significantly increase the cost while reducing the throughput. Therefore, there is a need for developing low temperature solution processing of metal oxide films starting from simple and low-cost commercially available precursors.

Here, we demonstrate that room temperature processing of simple solution formulation (titanium (IV) isopropoxide ($Ti(OiPr)_4$) in isopropanol) can result in a TiO_x layer with high performance in MHP solar cells, as evidenced by a champion solar cell efficiency of 16.3%. Using optical spectroscopy, electrical measurements and X-ray diffraction, we show that the room temperature processed TiO_x is amorphous with organic residues and yet their optical and electrical properties are on par with the high temperature TiO_2. Flexible MHP perovskite solar cells with a power conversion efficiency of 14.3% were achieved with the room temperature processed TiO_x layer. The power conversion efficiency could be potentially increased further through process optimization.

Results and Discussion

The room temperature processed thin films from $Ti(OiPr)_4$ solution, from here on referred to as "$Ti(OiPr)_4$ RT", were prepared on top of glass/indium-tin-oxide (ITO) substrates as described in the Methods section. The thickness of $Ti(OiPr)_4$ RT film was measured to be 20 nm using ellipsometry (Supplementary Table 1). Scanning electron microscopy (SEM) images show pin-hole free surface morphology (Supplementary Fig. 1). Hydrolysis and condensation of precursor $Ti(OiPr)_4$ is the key to forming solid thin film.[23] Once the $Ti(OiPr)_4$ precursor solution is spin coated on the ITO slide, the isopropanol solvent evaporates quickly and $Ti(OiPr)_4$ makes contact with moisture in the air. Subsequently, hydrolysis and condensation reactions form Ti-O-Ti linkages.[24] Incomplete condensation will result in OH group left in the thin film,[25] as is the case with our $Ti(OiPr)_4$ RT film (*vide infra*).

We fabricated and tested perovskite solar cells with $Ti(OiPr)_4$ RT films deposited in different relative humidity (RH) to investigate the impact of RH on solar cell efficiency. The device structure is shown in Figure 1a and 1b. On top of the $Ti(OiPr)_4$ RT film, methylammonium lead iodide ($MAPbI_3$) layer (~300 nm), spiro-OMeTAD (100 nm), and silver anode layer (60 nm) were deposited as described in the Methods section. The cells with $Ti(OiPr)_4$ RT films fabricated in 40% to 55% RH resulted in highest efficiency (Supplementary Fig. 2), so all the following $Ti(OiPr)_4$

films were made in 55% RH. Next, to check for the impact of thermal annealing on solar cell efficiency, $Ti(OiPr)_4$ films were annealed immediately after the spin-coating step at various temperatures in the range of room temperature up to 500 ºC. Our results show that the temperature at which the $Ti(OiPr)_4$ thin film is annealed has no significant impact on the solar cell efficiency (Figure 1c). Specifically, the unannealed film (room temperature) and 500 °C annealed films result in comparable open-circuit voltages (V_{oc}), short-circuit current densities (J_{sc}), fill factors (FF), and efficiencies (η) as shown in Fig. 1d.

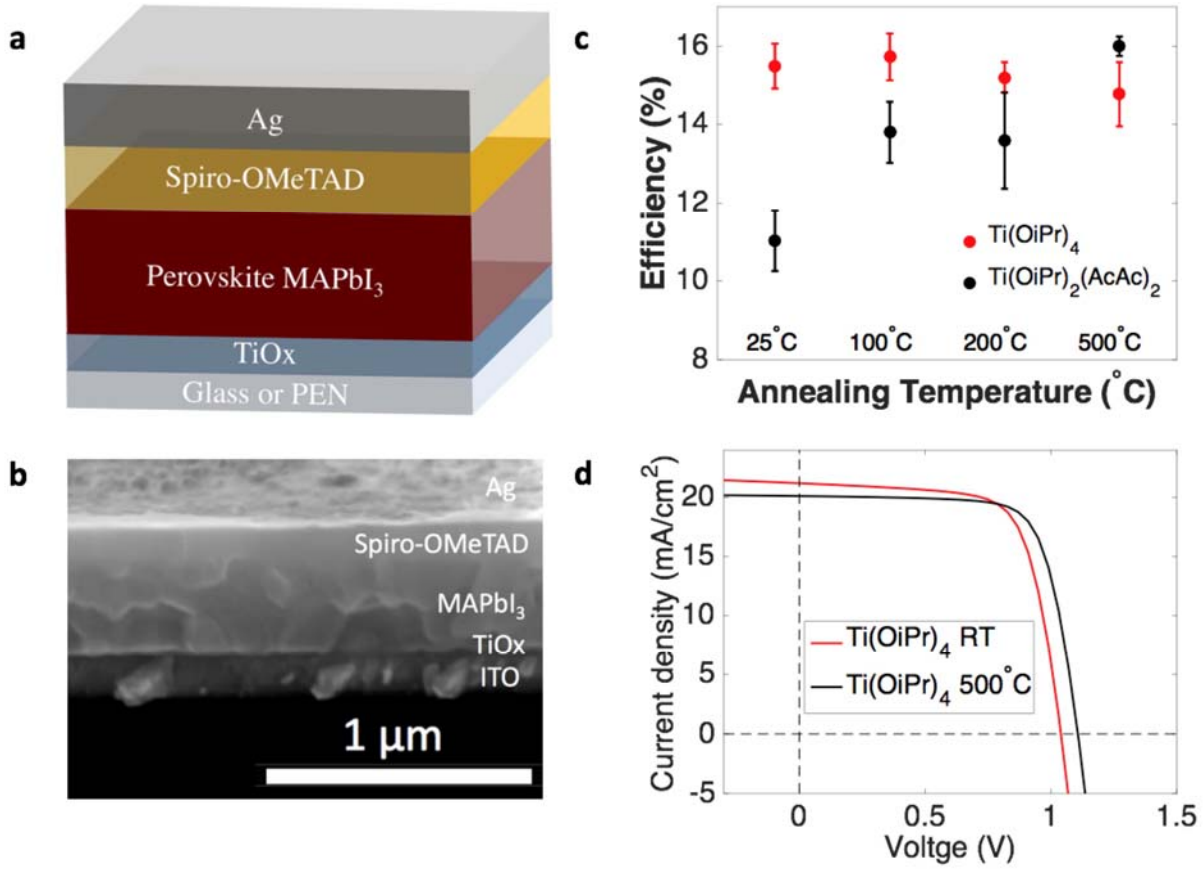

Figure 1: Device structure and their performance. (a) Perovskite solar cell structure. (b) SEM image of device cross-section. Scale bar represents 1µm. (c) Impact of annealing temperature of ETL to performance of solar cells when two different precursor solutions were used, $Ti(OiPr)_4$ and $Ti(OiPr)_2(AcAc)_2$. (d) J-V curve of champion cell with $Ti(OiPr)_4$ film without annealing and annealed at 500ºC.

Additionally, we examined the impact of thermal annealing temperature on the performance of TiO_2 thin films made from titanium diisopropoxide bis(acetylacetonate) in butanol, from here on referred to as "$Ti(OiPr)_2(AcAc)_2$". This is the most commonly employed TiO_2 precursor solution for high efficiency perovskite solar cells [26-28] and typically annealed at high temperatures (>450 °C). Our results show that, indeed, varying the annealing temperature from 25 °C to 500 °C, the solar cell efficiency changes from 11% to 16% (Figure 1c), mostly due to an increase in the short-circuit current density (Supplementary Fig. 3). We attribute the starkly

different dependence of $Ti(OiPr)_4$ and $Ti(OiPr)_2(AcAc)_2$ performance on the annealing temperature to slower hydrolysis of the acetylacetone groups.[29] $Ti(OiPr)_2(AcAc)_2$ has an octahedral coordination with two isopropoxide and two acetylacetone (AcAc) groups around a central titanium atom. Previous literature has shown that the labile isopropoxide groups can be easily hydrolyzed compared to AcAc groups.[29,30] In fact, the AcAc groups have been used to stabilize the solution formulation by suppressing uncontrolled precipitation since hydrolysis of the AcAc groups is significantly more suppressed.[31] Therefore, when ($Ti(OiPr)_2(AcAc)_2$) is used as precursor solution to form the titania ETL layer, pyrolysis at high temperature is needed rather than just hydrolysis. In contrast, we show in this work that $Ti(OiPr)_4$ can readily form a titania layer at room temperature that performs well in perovskite solar cells.

To better understand the nature of the $Ti(OiPr)_4$ RT film, we performed optical, electrical and X-ray diffraction characterization. The absorbance spectra of the $Ti(OiPr)_4$ RT film and $Ti(OiPr)_2(AcAc)_2$ 500 ºC film were measured using a spectrophotometer equipped with an integrating sphere (Figure 2a).The bandgap of $Ti(OiPr)_4$ RT film was determined to be 3.69 eV using a Tauc plot, which matches the band gap of TiO_x reported in the literature.[32,33] The absorbance onset of precursor $Ti(OiPr)_4$ solution is 3.89 eV which is higher than the deposited $Ti(OiPr)_4$ RT film. The band gap of $Ti(OiPr)_2(AcAc)_2$ 500 ^{o}C film was determined to be 3.57 eV, which is slightly lower than the band gap of the $Ti(OiPr)_4$ RT film. Fourier Transform Infrared (FT-IR) spectroscopy results are shown in Figure 2b. Both samples show absorption in the region below 1000 cm^{-1} which corresponds to vibration peak of Ti–O–Ti bonds,[25] suggesting that Ti-O-Ti bonds have formed in both cases.

In higher wavenumber regions, the spectrum from $Ti(OiPr)_4$ sample shows several peaks that are missing in the spectrum from $Ti(OiPr)_2(AcAc)_2$ sample. These peaks are associated with O-H groups (2450 – 3600 cm^{-1} and 1600 - 1700 cm^{-1}), C-O stretching (1050 -1180 cm^{-2}), C-H bending (1350 – 1410 cm^{-2}), and C-H stretching (2850 - 3000 cm^{-2}). These peaks indicate the presence of OH group as well as organic residues in the $Ti(OiPr)_4$ sample.[34] In a pH neutral condition such as $Ti(OiPr)_4$ in IPA, a significant fraction of the product will form weaker olation bonds, which consists of metal ions bridged through hydroxide, rather than condensation bonds.[35] FTIR spectra indicates the occurrence of a terminal type of OH groups,[25] which passivate the dangling bond of the TiO_x. Therefore, our FTIR results suggests that some of $Ti(OiPr)_4$ did not completely go through the hydrolysis and condensation steps.

X-ray diffraction (XRD) patterns show no peaks from thin films deposited from $Ti(OiPr)_4$ and annealed below 350 ºC (Figure 2d). If annealed at above 350 ºC, XRD patterns show peaks that correspond to anatase TiO_2. The transition temperature of ~350 ºC observed in our work is consistent with the transition from amorphous to anatase phase of TiO_2.[36] Our Raman spectroscopy results also present consistent picture that $Ti(OiPr)_4$ RT sample is completely amorphous since there is no obvious peaks that correspond to crystalline TiO_2 as shown previously in the literature[37] (Figure 2c). In comparison, $Ti(OiPr)_2(AcAc)_2$ 500 ºC show peaks at 141, 398, 516, and 640 cm^{-1} Raman shift that correspond agreeably to anatase phase of TiO_2.[37]

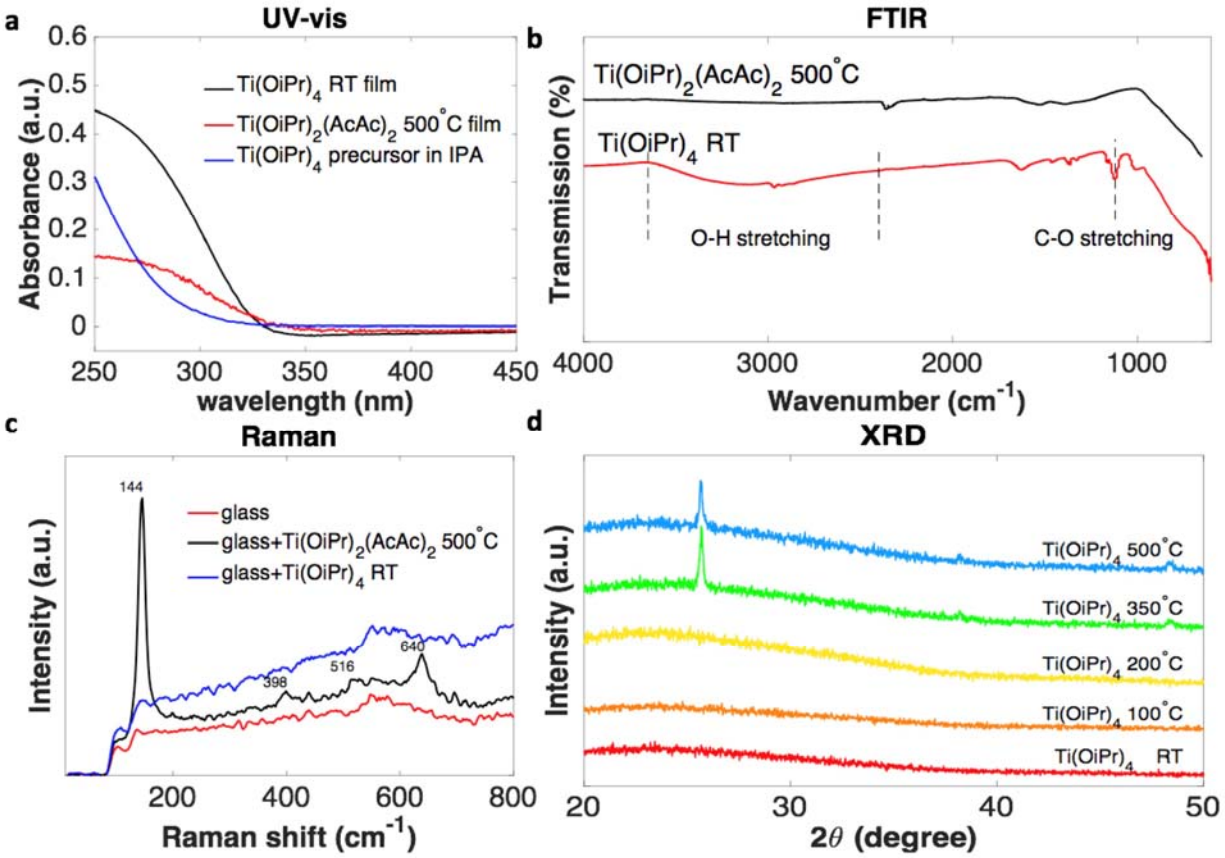

Figure 2: Characterization for $Ti(OiPr)_4$ film. (a) UV-vis absorbance spectra for $Ti(OiPr)_4$ RT film, $Ti(OiPr)_2(AcAc)_2$ 500 ºC film and $Ti(OiPr)_4$ RT precursor solution. (b) FTIR transmission spectra of $Ti(OiPr)_2(AcAc)_2$ 500ºC and $Ti(OiPr)_4$ powder. (c)Raman spectra of substrate glass, $Ti(OiPr)_4$ RT film and $Ti(OiPr)_2(AcAc)_2$ 500 ºC film. (d) XRD of $Ti(OiPr)_4$ film without annealing, annealed at 100 ºC, 200 ºC, 350 ºC and 500 ºC.

The electrical resistivity was determined using a two-terminal measurement with ITO and thermally evaporated silver as the electrical contacts with TiO_x thin film sandwiched in the middle. The measured resistivity for the TiO_x thin films annealed at different temperatures are shown in Table 1. They are in the range of $60 \sim 150 \times 10^5$ Ω·cm which lies between that of metals (10^{-6} Ω cm) and insulators (10^{14} Ω cm), indicating semiconducting behavior. TiO_2 has a resistivity of 10^8 Ω cm making it electrically insulating, but as the titanium ratio increases relative to the oxide it becomes more like an n-type semiconductor and its resistivity decreases.[38] This indicates that our film is partially suboxidized due to the resistivity being 3 orders of magnitude lower than pure TiO_2. This indicates that the titanium/oxygen ratio in our films will drastically affect our electrical properties.[38] As the film is annealed at higher temperatures, the observed slight increase in two-terminal resistivity is likely due to the increase in sheet resistance of ITO thin films at temperatures greater than 300 °C. Our TiO_x resistivity measurements are on the same order of magnitude as those obtained from magnetron sputtering at varying substrate temperatures by Su *et al.*[9] Additionally, this high resistivity ensures us that our film is complete and pinhole-free, otherwise short paths would arise and dramatically reduce the measured resistance.

Table 1 Electrical resistivity of TiO_x thin films prepared from $Ti(OiPr)_4$ solution

Anneal Temp (°C)	Two Terminal Resistivity (10^5 Ω·cm)
25	61.88
110	78.75
300	101.3
500	144.0

Refractive indices of the $Ti(OiPr)_4$ and $Ti(OiPr)_2(AcAc)_2$ thin films prepared at room temperature, and annealed at 110 °C, and 500 °C on ITO coated glass were measured using ellipsometry (Supplementary Figure 5). The measured spectral refractive were obtained in the range of 250 - 750 nm. At 633 nm, our films have refractive index of 1.75, which is much lower than the value of anatase TiO_2 (2.55)[39], but more close to amorphous TiO_2 (2.03)[39]. This is consistent with our Raman, XRD and FTIR results that indicate our film being amorphous TiO_x. The lower refractive indices also indicate that the $Ti(OiPr)_4$ thin films processed at room temperature may be a low density film with organic residues as shown by FTIR. The refractive index of TiO_2 is known to correlate positively with annealing temperature and titanium oxide density.[40,41]

By employing the room temperature processed TiO_x layer, we have fabricated and tested flexible perovskite solar cells using ITO-coated PEN substrates (Figure 3). The device architecture is shown in Figure 1a. The champion device achieved 14.3% efficiency, with J_{sc} of 20.04 mA/cm^2, V_{oc} of 1.00 V, FF of 73.42% (Figure 3b). This is close to the record for efficiency of flexible solar cell based on $MAPbI_3$, 15% to 16%. The highest record efficiency so far by Wang *et.* of 18% efficiency has been achieved with alloyed perovskites.[6] We emphasize that all of these previous record efficiency results have relied on either vacuum processing (ALD or sputter deposition) or colloidal nanoparticles whereas our flexible solar cells are based on room temperature and non-vacuum processing with simple sol-gel precursor. To check for the stability of our flexible solar cells, we monitored the device performance over a time period in nitrogen glovebox storage and found that the device maintained ~90% of its original efficiency after two weeks (Supplementary Figure 6). We have also performed mechanical durability testing by bending the device with a radius of curvature of 5 mm (Supplementary Figure 7). After 300 bending cycles, the device maintained ~85% of its original efficiency. The decrease in efficiency was caused mainly by the reduced J_{SC} and increased series resistance.

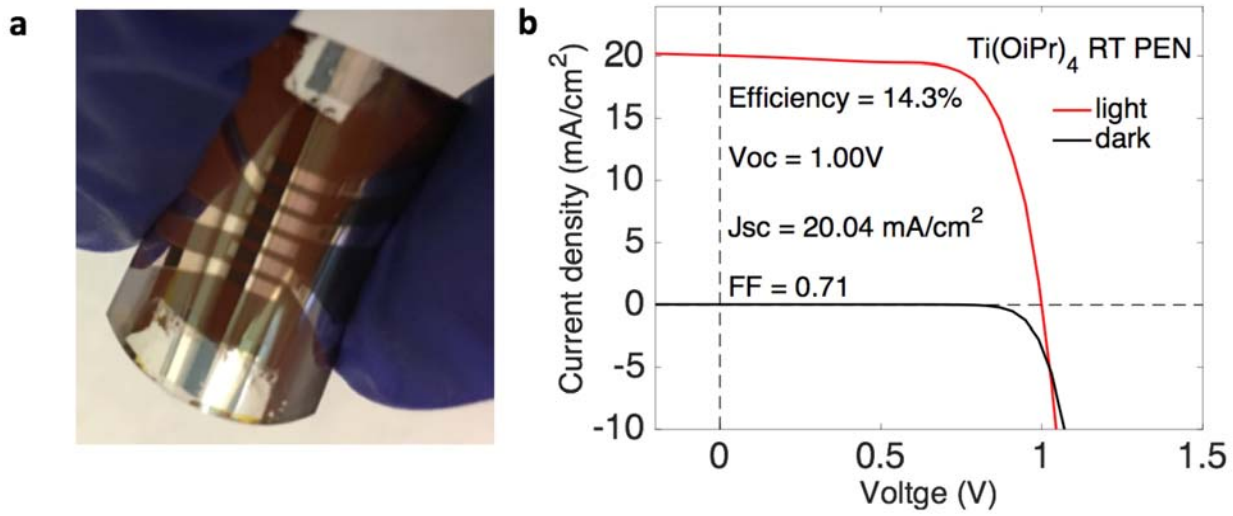

Figure 3: flexible solar cell. (a) Picture of flexible perovskite solar cell and (b) J–V curves for device fabricated on ITO-covered PEN. Efficiency, FF, V_{oc} (V) and J_{sc} (mA/cm^{-2}) are shown in inset.

In summary, we demonstrated room temperature solution processing of amorphous TiO_x thin film with high performance TiO_x ETL in MHP solar cells. We showed that the solar cell efficiency with the TiO_x films annealed at temperature in the range of room temperature to 500 ºC is similar, suggesting that thermal annealing at high temperature is not necessary to achieve high solar cell performance. Flexible MHP solar cells that employ the room temperature processed TiO_x layer achieved a PCE of 14.3% and show promising stability and mechanical durability. Our work highlights the potential of flexible, lightweight and high efficiency MHP solar cells fabricated all through low-cost, high-throughput and low thermal budget processing steps.

Methods

$Ti(OiPr)_4$ RT film

Our TiO_x solution was prepared using a method adapted from Back *et al*,[42] Titanium (IV) isopropoxide ($Ti(OiPr)_4$) was purchased from Sigma Aldrich and prepared in a 1:50 volume ratio with isopropanol (IPA), which contains 0.02% H_2O. The solution is ready to use immediately without heating. The $Ti(OiPr)_4$ solution was spin-coated onto indium-tin-oxide (ITO) patterned glass at 3000 rpm for 30 seconds. Compact TiO_2 thin films were fabricated by spin coating a solution of 146.6 µL $Ti(OiPr)_2(AcAc)_2$ in 2 mL of butanol for 30 s at 4000 rpm and annealing at 450 ºC for 5 minutes.

Solar cell fabrication

The patterned ITO glass substrate was cleaned sequentially in Hellmanex 3 detergent, deionized water, and ethanol in an ultrasonic cleaner, rinsed with acetone and IPA, and placed in ultraviolet ozone plasma cleaner for 5 minutes. The patterned ITO glass and PEN substrates (25.4 mm^2) were purchased from Kintec Company. Scotch tape was used to cover the end of the ITO contact to protect it from being coated during spin coating. $Ti(OiPr)_4$ RT film was deposited on ITO slides.

$MAPbI_3$ was prepared using an adapted inter-diffusion method from Xiao et al[43]. 1M PbI_2 (99.9985%) and dimethyl sulfoxide (DMSO) (anhydrous, Sigma-Aldrich) were dissolved in dimethylformamide (DMF) (anhydrous, Sigma-Aldrich) and stirred for 2 hours at 60 ºC. Methylammonium iodide (MAI) (Dyesol) was dissolved in IPA (anhydrous, Sigma-Aldrich) at 50 mg/mL concentration. Next, the PbI_2 and MAI solutions were spin coated at 2000 rpm for 1 minute sequentially and annealed at 110 °C for 12 minutes in a nitrogen filled glovebox. (2,2′,7,7′-tetrakis N, N-di-p-methoxyphenylamine)-9,9′-spirobi- fluorine (Spiro-OMeTAD, Luminescence Technology Corp.) was dissolved at a 72 mg/mL concentration in chlorobenzene. It was doped with 28.8 µL of a 520 mg/mL solution of 4-tert-butylpuridine in acetronile and 17.5 µL of a 520 mg/mL solution of lithium bis(trifluoromethylsulphonyl)imide in acetonitrile. The Spiro-OMeTAD solution was spin-coated at 4000 rpm for 30 seconds in a nitrogen filled glovebox and left to oxidized in a dry air overnight. The rear silver (Ag) contact was prepared by thermally evaporating 60 nm of silver at a vacuum of $1x10^{-6}$ mbar. Silver evaporation pellets (99.999%) were purchased from Kurt J. Lesker company. The complete device structure is shown in Figure 1b.

Characterization

Solar cell characterization: The devices were tested using a Keithley source-meter operating at a scan rate of 1 V/s under AM 1.5 illumination from a solar simulator (PV Measurements). Calibration of the light source was done using a reference silicon solar cell and current and height adjustments (PV Measurements). While testing, an optical mask was used to only expose the 0.03 cm^2 active device area.

UV-Vis: UV-Vis spectra of the TiO_x with quartz as substrate was done with a UV/Vis/NIR Lambda 950 S spectrometer from Perkin Elmer. Integrating sphere was used and absorbance of film has been calculated by 100%-Transmission-Reflection. Band gaps were calculated using the Tauc plot method with indirect band gap power factor.

FT-IR: FT-IR transmission spectra of liquids and powders were collected with a Thermo Scientific Nicolet 6700 FT-IR with MCT/A detector and a SenseIR Technologies DuraScope ATR operating between 650-4000 cm^{-1}.

Raman spectroscopy: Raman spectra were taken on Remishaw inVia Raman Microscope using an excitation source with a wavelength of 514 nm.

X-ray diffraction: X-ray diffraction spectra were taken with a PANalytical X'Pert Pro MPD XRD with a Cu source operating at 40 kV and 40 mA. All measurements are performed at room temperature.

SEM: Planar and cross-sectional SEM images were captured with an FEI Quanta 650 SEM operating between 5kV and 15kV accelerating voltage.

Electrical resistivity: Electrical resistivity was measured using a two terminal method that had ITO and evaporated silver as the electrical contacts at both ends and TiO_x in the middle. A Fluke 289 True RMS Multimeter was used to measure the resistance and resistivity was calculated from the contact area. Copper tape was used to prevent punch through by the probe. A Jandel Four Point Probe was used to verify sheet resistances of the ITO coated glass substrate.

Ellipsometry: Film thickness and refractive index was calculated using a Horiba Jobin Yvon UVISEL Vis ellipsometer and DeltaPsi2 modeling. Spectroscopic elliposmetry was collected between 250 to 750 nm at a 70° angle of incidence with the modulator and analyzer at 0° and 45°, respectively. A TiO_2 dispersion file was used to model the spectra of TiO_x thin film. Interfacial regions and surface roughness was accounted for in the modeling.

Acknowledgement

J. J. C. acknowledges support from an Early Career Faculty Award grant from NASA's Space Technology Research Grants Program (NNX15AU43G). M. C. G. acknowledges support from the NASA Langley Professor Program and IRAD.

Supplementary Information

Room temperature processing of TiO_x electron transporting layer for perovskite solar cells

Xiaoyu Deng[1a], George C. Wilkes[2a], Alexander Z. Chen, Narasimha S. Prasad[3], Mool C. Gupta [2b], Joshua J. Choi[1b]

4. Department of Chemical Engineering, University of Virginia, Charlottesville, Virginia 22904, USA
5. Department of Electrical and Computer Engineering, University of Virginia, Charlottesville, Virginia 22904, USA
6. NASA Langley Research Center, Hampton, VA 23666

c. These authors contributed equally to this work

d. Correspondence and requests for materials should be addressed to J. J. C and M. C. G. (email: jjc6z@virginia.edu; mgupta@virginia.edu)

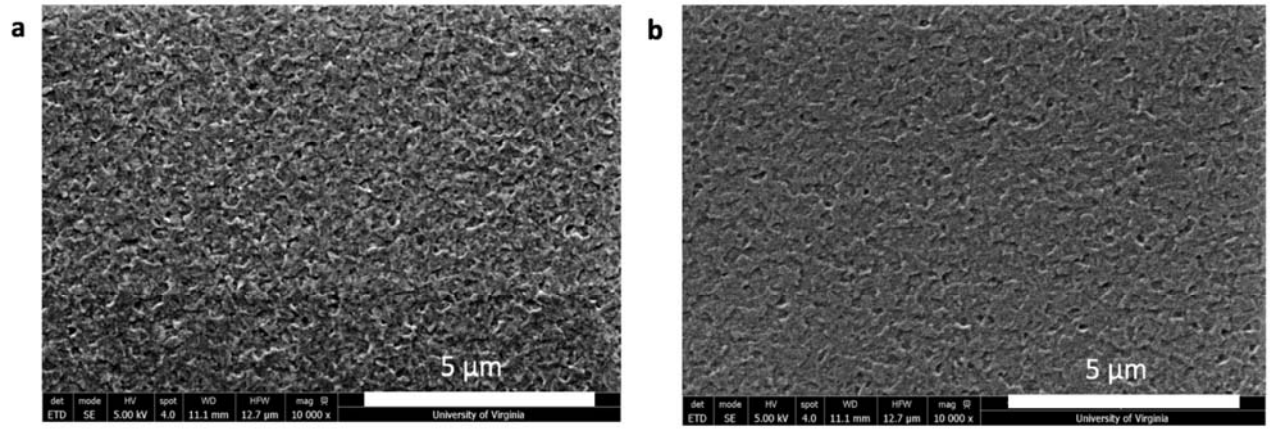

Supplementary Figure 1. Topographical SEM images of (a) ITO surface and (b) TiO_x film on top of ITO formed by spin-coating $Ti(OiPr)_4$ precursor solution. Images were taken at 5kV accelerating voltage.

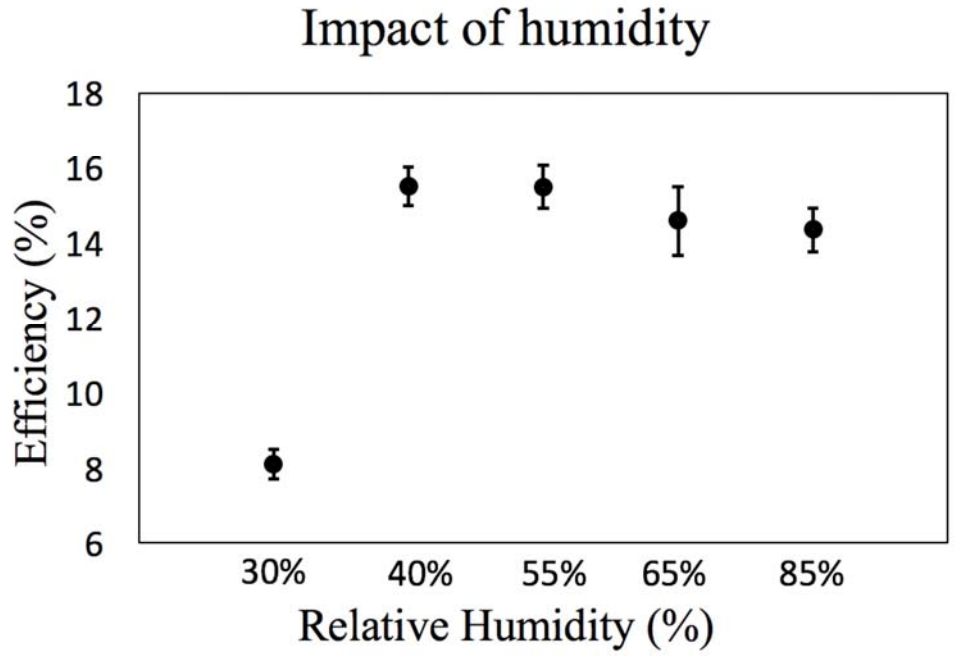

Supplementary Figure 2. Impact of humidity on performance of fabricated solar cells

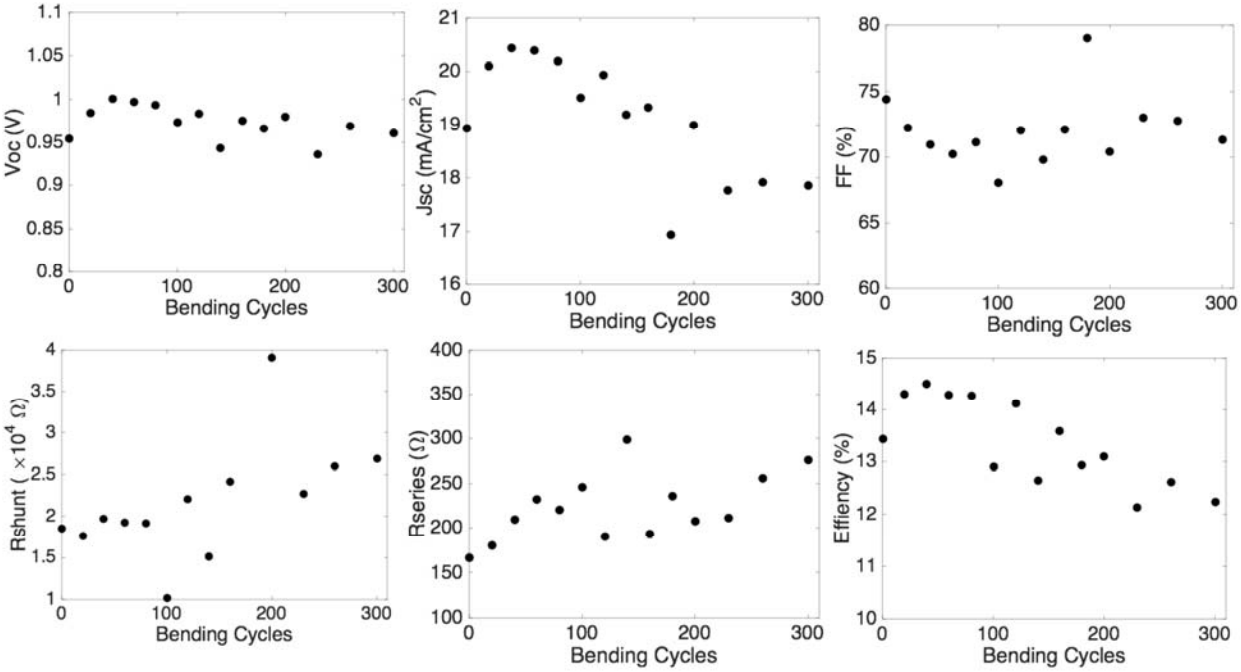

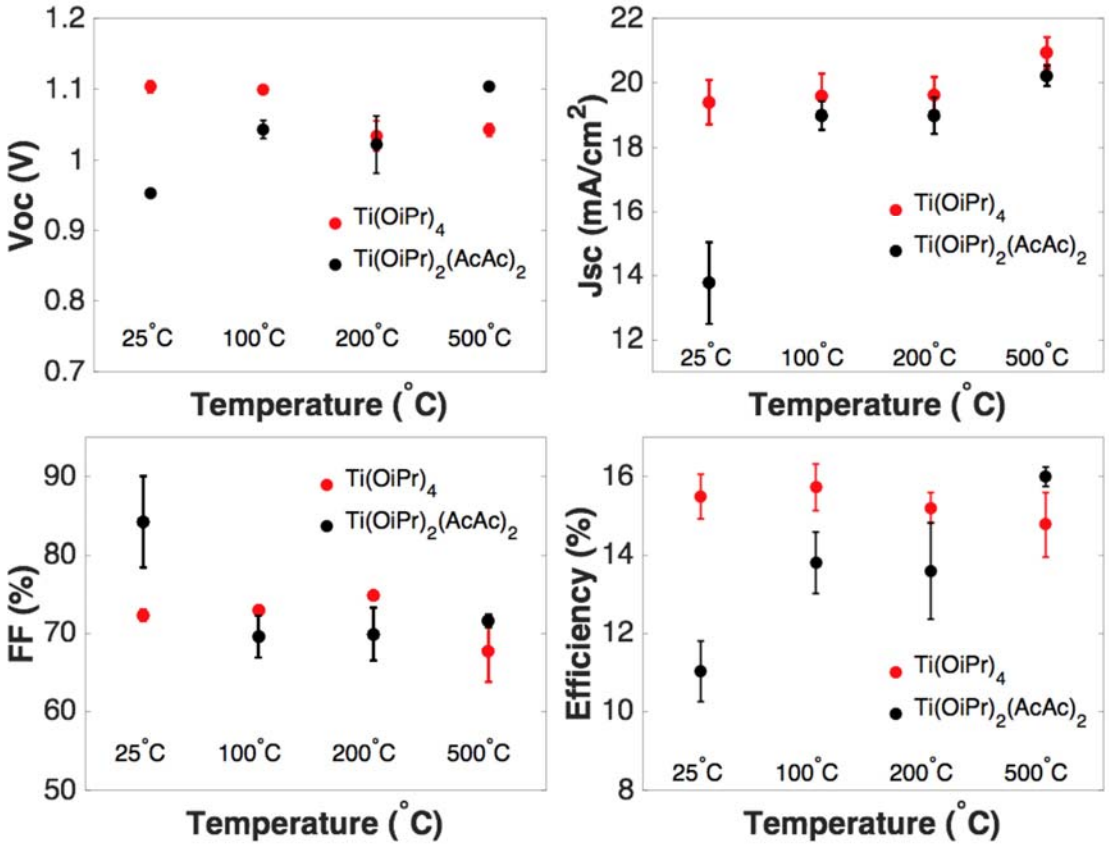

Supplementary Figure 3. Impact of annealing temperature to J_{SC}, V_{OC}, FF and efficiency of solar cells with ETL made from two different precursor solutions. The temperature range is RT to 500ºC.

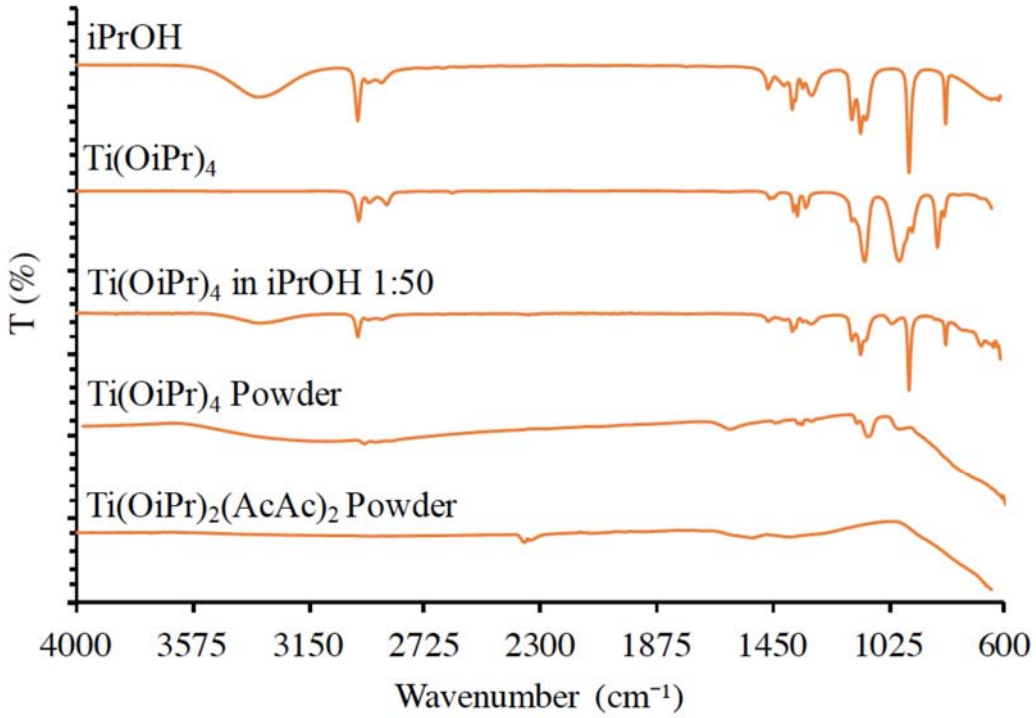

Supplementary Figure 4. FT-IR transmission spectra of IPA, $Ti(OiPr)_4$, diluted $Ti(OiPr)_4$, $Ti(OiPr)_4$ powder and $Ti(OiPr)_2(AcAc)_2$ powder.

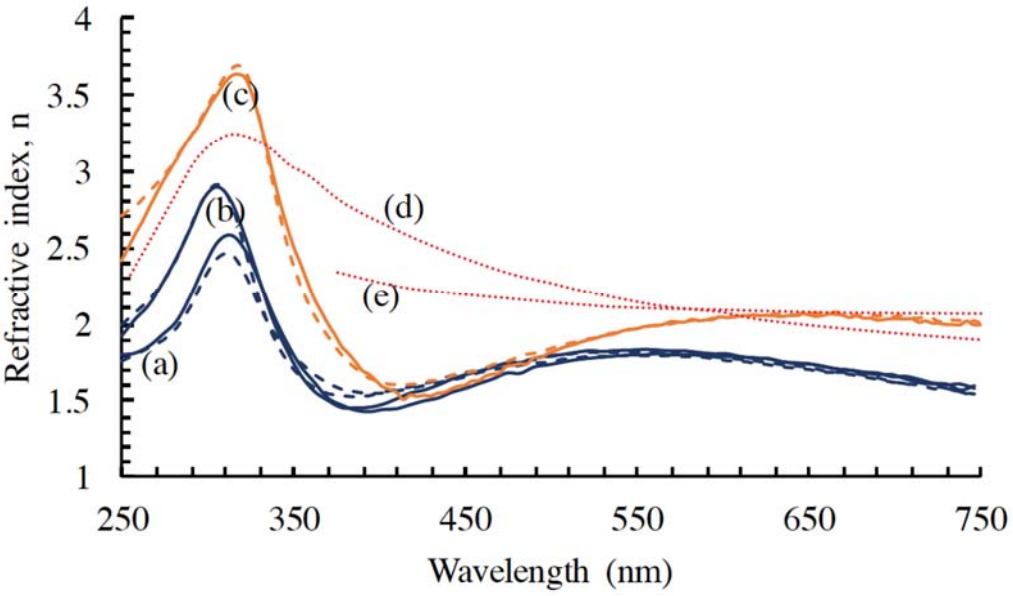

Supplementary Figure 5. Spectral refractive indices for the $Ti(OiPr)_4$ (Blue) and $Ti(OiPr)_2(AcAc)_2$ (Orange) thin films prepared (a) at room temperature, and annealed at (b) 110°C, and (c) 500°C on ITO coated glass. Solid lines indicate data measured from the ellipsometer, while the dashed lines indicate modeled data from DeltaPsi2. Additionally, spectral refractive indices of

amorphous (d) and nano crystalline (e) TiO_2 films were obtained from Akimov and Tauson and are overlaid as red dotted lines.

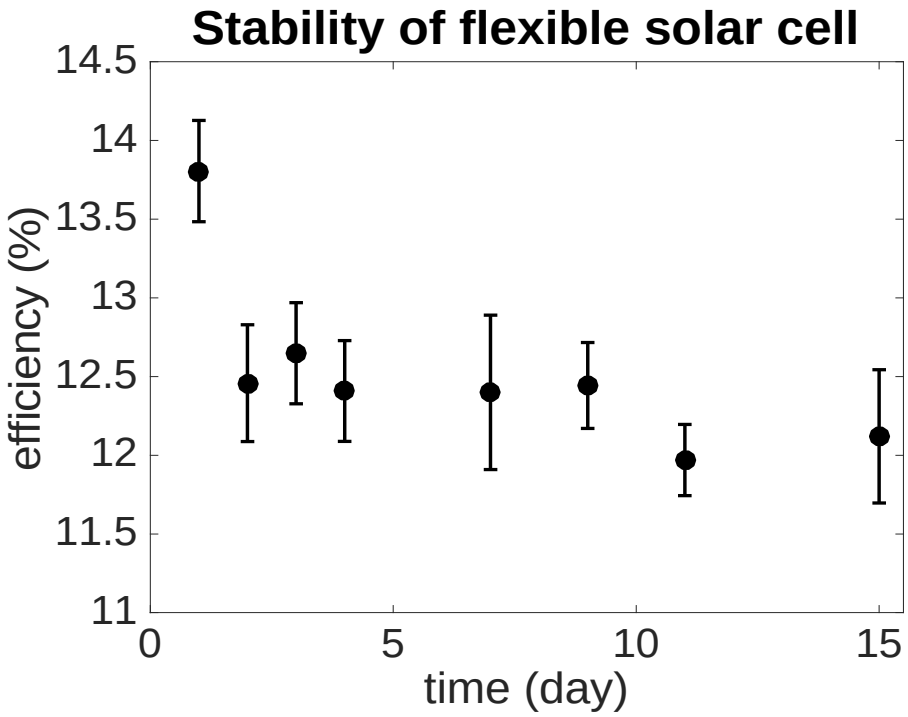

Supplementary Figure 6. Stability of flexible solar cell as a function of storage time in nitrogen glovebox.

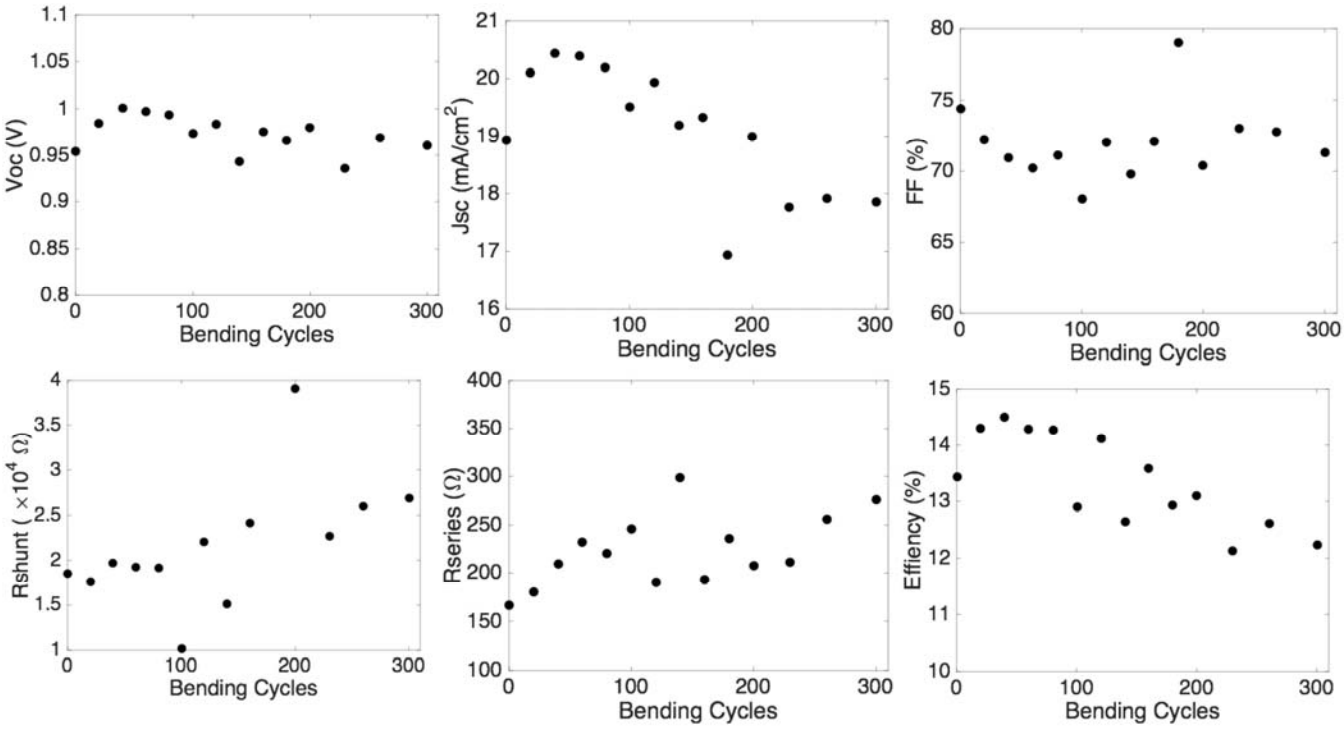

Supplementary Figure 7. Flexible solar cell performance as a function of bending cycles

Supplementary Table 1. TiO_x film thickness measured from ellipsometry in nanometers

Sample	Interfacial	Film	Roughness	Overall
$Ti(OiPr)_4$ 25°C	0.000 ± 0.113	20.322 ± 1.233	0.796 ± 0.742	21.118 ± 2.088
$Ti(OiPr)_4$ 110°C	0.000 ± 0.077	15.509 ± 1.575	2.029 ± 1.069	17.538 ± 2.721
$Ti(OiPr)_2(AcAc)_2$ 500°C	0.000 ± 0.082	16.636 ± 1.107	1.649 ± 0.769	18.285 ± 1.958

Reference

1 NREL 2014, [online] Available: http://www.nrel.gov/ncpv/images/efficiency_chart.jpg

2 Di Giacomo, F., Fakharuddin, A., Jose, R. and Brown, T. M. Progress, challenges and perspectives in flexible perovskite solar cells. *Energy Environ. Sci.* **9**, 3007-3035 (2016).

3 Samuel D. Stranks, G. E. E., Giulia Grancini, Christopher Menelaou, Marcelo J. P. Alcocer, Tomas Leijtens. Electron-Hole Diffusion Lengths Exceeding 1 Micrometer in an Organometal Trihalide Perovskite Absorber. *Science* **342**, 341-344 (2013).

4 Mali, S. S., Hong, C. K., Inamdar, A. I., Im, H. and Shim, S. E. Efficient planar n-i-p type heterojunction flexible perovskite solar cells with sputtered TiO2 electron transporting layers. *Nanoscale* **9**, 3095-3104 (2017).

5 Heo, J. H., Lee, M. H., Han, H. J., Patil, B. R., Yu, J. S. and Im, S. H. Highly efficient low temperature solution processable planar type CH3NH3PbI3perovskite flexible solar cells. *J. Mater. Chem. A* **4**, 1572-1578 (2016).

6 Changlei Wanga, D. Z., Yue Yub, Niraj Shresthab, Corey R. Griceb, Weiqiang Liaob, Alexander J. Cimarolib, Jing Chenc, Randy J. Ellingsonb, Xingzhong Zhaoa, Yanfa Yan. Compositional and morphological engineering of mixed cation perovskite films for highly efficient planar and flexible solar cells with reduced hysteresis. *Nano Energy* **35**, 223-232 (2017).

7 Wojciechowski, K., Saliba, M., Leijtens, T., Abate, A. and Snaith, H. J. Sub-150 °C processed meso-superstructured perovskite solar cells with enhanced efficiency. *Energy Environ. Sci.* **7**, 1142-1147 (2014).

8 Yella, A., Heiniger, L. P., Gao, P., Nazeeruddin, M. K. and Gratzel, M. Nanocrystalline rutile electron extraction layer enables low-temperature solution processed perovskite photovoltaics with 13.7% efficiency. *Nano Lett* **14**, 2591-2596 (2014).

9 Su, H. X., Peng, Z. J. and Fu, X. L. Composition, Structure and Electrical Resistivity of TiOx Thin Films Deposited by RF Magnetron Sputtering at Varied Substrate Temperatures. *Key Engineering Materials* **602-603**, 1039-1042 (2014).

10 Dkhissi, Y., Huang, F., Rubanov, S., Xiao, M., Bach, U., Spiccia, L., Caruso, R. A. and Cheng, Y.-B. Low temperature processing of flexible planar perovskite solar cells with efficiency over 10%. *Journal of Power Sources* **278**, 325-331 (2015).
11 Das, S., Gu, G., Joshi, P. C., Yang, B., Aytug, T., Rouleau, C. M., Geohegan, D. B. and Xiao, K. Low thermal budget, photonic-cured compact TiO2layers for high-efficiency perovskite solar cells. *J. Mater. Chem. A* **4**, 9685-9690 (2016).
12 Dianyi Liu, T. L. K. Perovskite solar cells with a planar heterojunction structure prepared using room-temperature solution processing techniques. *Nature Photonics* **8**, 133-138 (2014).
13 Shin, S. S., Yang, W. S., Noh, J. H., Suk, J. H., Jeon, N. J., Park, J. H., Kim, J. S., Seong, W. M. and Seok, S. I. High-performance flexible perovskite solar cells exploiting Zn2SnO4 prepared in solution below 100 degrees C. *Nat Commun* **6**, 7410 (2015).
14 Yang, D., Yang, R., Zhang, J., Yang, Z., Liu, S. and Li, C. High efficiency flexible perovskite solar cells using superior low temperature TiO2. *Energy Environ. Sci.* **8**, 3208-3214 (2015).
15 Atsushi Kogo, S. I., Masashi Ikegami, and Tsutomu Miyasaka. An Ultrathin Sputtered TiO2 Compact Layer for Mesoporous Brookite-based Plastic CH3NH3PbI3−xClx Solar Cells. *Chemistry Letters* **46**, 530-532 (2017).
16 Huang, A., Zhu, J., Zhou, Y., Yu, Y., Liu, Y., Yang, S., Ji, S., Lei, L. and Jin, P. One step spray-coated TiO2 electron-transport layers for decent perovskite solar cells on large and flexible substrates. *Nanotechnology* **28**, 01LT02 (2017).
17 Zhou, P., Li, W., Li, T., Bu, T., Liu, X., Li, J., He, J., Chen, R., Li, K., Zhao, J. and Huang, F. Ultrasonic Spray-Coating of Large-Scale TiO2 Compact Layer for Efficient Flexible Perovskite Solar Cells. *Micromachines* **8**, 55 (2017).
18 Qiu, W., Paetzold, U. W., Gehlhaar, R., Smirnov, V., Boyen, H.-G., Tait, J. G., Conings, B., Zhang, W., Nielsen, C. B., McCulloch, I., Froyen, L., Heremans, P. and Cheyns, D. An electron beam evaporated TiO2layer for high efficiency planar perovskite solar cells on flexible polyethylene terephthalate substrates. *J. Mater. Chem. A* **3**, 22824-22829 (2015).
19 Chandiran, A. K., Yella, A., Mayer, M. T., Gao, P., Nazeeruddin, M. K. and Gratzel, M. Sub-nanometer conformal TiO(2) blocking layer for high efficiency solid-state perovskite absorber solar cells. *Adv Mater* **26**, 4309-4312 (2014).
20 Kim, B. J., Kim, D. H., Lee, Y.-Y., Shin, H.-W., Han, G. S., Hong, J. S., Mahmood, K., Ahn, T. K., Joo, Y.-C., Hong, K. S., Park, N.-G., Lee, S. and Jung, H. S. Highly efficient and bending durable perovskite solar cells: toward a wearable power source. *Energy Environ. Sci.* **8**, 916-921 (2015).
21 Chen, J.-Y., Chueh, C.-C., Zhu, Z., Chen, W.-C. and Jen, A. K. Y. Low-temperature electrodeposited crystalline SnO 2 as an efficient electron-transporting layer for conventional perovskite solar cells. *Solar Energy Materials and Solar Cells* **164**, 47-55 (2017).
22 Zhang, J., Juárez-Pérez, E. J., Mora-Seró, I., Viana, B. and Pauporté, T. Fast and low temperature growth of electron transport layers for efficient perovskite solar cells. *J. Mater. Chem. A* **3**, 4909-4915 (2015).
23 Danks, A. E., Hall, S. R. and Schnepp, Z. The evolution of 'sol–gel' chemistry as a technique for materials synthesis. *Mater. Horiz.* **3**, 91-112 (2016).

24 Park, S. H., Roy, A., Beaupré, S., Cho, S., Coates, N., Moon, J. S., Moses, D., Leclerc, M., Lee, K. and Heeger, A. J. Bulk heterojunction solar cells with internal quantum efficiency approaching 100%. *Nature Photonics* **3**, 297-302 (2009).

25 Nakamura, M., Kato, S., Aoki, T., Sirghi, L. and Hatanaka, Y. Role of terminal OH groups on the electrical and hydrophilic properties of hydro-oxygenated amorphous TiOx:OH thin films. *Journal of Applied Physics* **90**, 3391-3395 (2001).

26 Jeon, N. J., Noh, J. H., Yang, W. S., Kim, Y. C., Ryu, S., Seo, J. and Seok, S. I. Compositional engineering of perovskite materials for high-performance solar cells. *Nature* **517**, 476-480 (2015).

27 Liu, M., Johnston, M. B. and Snaith, H. J. Efficient planar heterojunction perovskite solar cells by vapour deposition. *Nature* **501**, 395-398 (2013).

28 Dongqin Bi, W. T., M. Ibrahim Dar, Peng Gao, Jingshan Luo, Clémentine Renevier, Kurt Schenk, Antonio Abate, Jean-David Decoppet, Shaik Mohammed Zakeeruddin, Mohammad Khaja Nazeeruddin, Michael Grätzel and Anders Hagfeldt. Efficient luminescent solar cells based on tailored mixed-cation perovskites. *Science Advances* **2**, e1501170 (2016).

29 C. SANCHEZ, J. L., M. HENRY and F. BABONNEAU Chemical Modification of Alkoxide Precursors. *Journal of Non-Crystalline Solids* **100**, 65-76 (1988).

30 K.G. CAULTON, L. G. H.-P. Synthesis, Structural Principles, and Reactivity of Heterometallic Alkoxides *chemical reviews* **90**, 969-995 (1990).

31 Duoss, E. B., Twardowski, M. and Lewis, J. A. Sol-Gel Inks for Direct-Write Assembly of Functional Oxides. *Advanced Materials* **19**, 3485-3489 (2007).

32 Jin Young Kim, K. L., Nelson E. Coates, Daniel Moses, Thuc-Quyen Nguyen, Mark Dante. Efficient Tandem Polymer Solar Cells Fabricated by All-Solution Processing. *Science* **317**, 222-225 (2007).

33 Masatoshi Nakamuraa, D. K., Toru Aokib, Jurgen Engemanna, Yoshinori Hatanakaa. Characterization of TiOx film prepared by plasma enhanced chemical vapor deposition using a multi-jet hollow cathode plasma source. *Applied Surface Science* **175-176**, 697-702 (2001).

34 Yi Wang, Y. Q., Guicun Li, Zuolin Cui, Zhikun Zhang. One-step synthesis and optical properties of blue titanium suboxide nanoparticles. *Journal of Crystal Growth* **282**, 402-406 (2005).

35 Kallala, M., Sanchez, C. and Cabane, B. Structures of inorganic polymers in sol-gel processes based on titanium oxide. *Physical Review E* **48**, 3692-3704 (1993).

36 Khatim, O., Amamra, M., Chhor, K., Bell, A. M. T., Novikov, D., Vrel, D. and Kanaev, A. Amorphous–anatase phase transition in single immobilized TiO2 nanoparticles. *Chemical Physics Letters* **558**, 53-56 (2013).

37 Ji, Y. Growth mechanism and photocatalytic performance of double-walled and bamboo-type TiO2nanotube arrays. *RSC Adv.* **4**, 40474-40481 (2014).

38 Yongfeng Ju, M. W., Yunlong Wang, Shihu Wang, and Chengfang Fu. Electrical Properties of Amorphous Titanium Oxide Thin Films for Bolometric Application. *Advances in Condensed Matter Physics* **2013** (2013).

39 Loper, P., Stuckelberger, M., Niesen, B., Werner, J., Filipic, M., Moon, S. J., Yum, J. H., Topic, M., De Wolf, S. and Ballif, C. Complex Refractive Index Spectra of CH3NH3PbI3 Perovskite Thin Films Determined by Spectroscopic Ellipsometry and Spectrophotometry. *J Phys Chem Lett* **6**, 66-71 (2015).

40 O. Ayieko, C., J. Musembi, R., M. Waita, S., O. Aduda, B. and K. Jain, P. Structural and Optical Characterization of Nitrogen-doped TiO2 Thin Films Deposited by Spray Pyrolysis on Fluorine Doped Tin Oxide (FTO) Coated Glass Slides. *International Journal of Energy and Engineering* **2**, 67-72 (2012).

41 D Mergela, D. B., S Eggerta, R Grammesb, B Samsetc. Density and refractive index of TiO2 films prepared by reactive evaporation. *Thin Solid Films* **371**, 218-224 (2000).

42 Back, H., Kim, G., Kim, J., Kong, J., Kim, T. K., Kang, H., Kim, H., Lee, J., Lee, S. and Lee, K. Achieving long-term stable perovskite solar cells via ion neutralization. *Energy Environ. Sci.* **9**, 1258-1263 (2016).

43 Xiao, Z., Dong, Q., Bi, C., Shao, Y., Yuan, Y. and Huang, J. Solvent annealing of perovskite-induced crystal growth for photovoltaic-device efficiency enhancement. *Adv Mater* **26**, 6503-6509 (2014).